AIAA JOURNAL
Vol. 37, No. 11, November 1999

Nonlinear Dynamic Finite Element Analysis of Composite Cylindrical Shells Considering Large Rotations

L. N. B. Gummadi* and A. N. Palazotto†
Air Force Institute of Technology, Wright–Patterson Air Force Base, Ohio 45433-6583

A new nonlinear finite element formulation is developed for the nonlinear dynamics of shell structures. Using a vectorial approach, the kinematics that can be used to describe very large displacements and large rotations are derived. Green strain measures and second Piola Kirchhoff stress measures are used in the determination of the total potential. A displacement-based eight-noded cylindrical shell element with a total of 36 degrees of freedom is developed. Several numerical examples are dynamically analyzed to observe the characteristics of large displacements and large rotations. A convergence study was carried out to establish the numerical accuracy of the model. The most efficient and accurate model was used.

Introduction

THE nonlinear vibration analysis of shells has been the focus of research for the past few years. Thin shells subjected to dynamic loads could encounter deflections of the order of the thickness of the shell. Dynamic response of thin shells also could lead to the phenomena of dynamic snapping or dynamic buckling. Because these kinds of responses cannot be determined accurately using small displacement and small rotation theories, large deformation and large rotation theories are required. The complex nature of these theories requires solving numerous simultaneous, nonlinear, differential equations. Even with simplifying assumptions, these equations remain complex and extensive.

As background, a few relevant past efforts are reviewed. Earlier work regarding the nonlinear vibrations for isotropic shell structures can be attributed to Carr,[1] Yeh,[2] Clough and Wilson,[3] Belytschko and Marchertas,[4] and Belytschko and Tsay.[5] These researchers used flat plate elements. Saigal and Yang[6] developed a curved shell element for isotropic shells. For composite shell structures, Simitses[7] provided an elegant analytical solution of thin laminated shells subjected to sudden loads. He ignored through-the-thickness shear effects and used Donnell-type kinematic relations. Raouf and Palazotto[8,9] developed a perturbation procedure to derive a set of asymptotically consistent nonlinear equations of motion for an arbitrary laminated composite cylindrical shell in cylindrical bending. They also neglected transverse shear effects. Simo and Tarnow[10] developed an energy and momentum conservating algorithm for shell analysis to analyze shells undergoing large rigid-body motions.

Palazotto and Dennis[11] presented the simplified large rotation (SLR) theory to analyze shells experiencing moderately large rotations. The SLR theory determines the equilibrium path of orthotropic shells using a total Lagrangian approach and includes a parabolic transverse shear stress distribution. This approach captures the appropriate kinematics through displacement polynomials. Green strain displacement relations are used, and all of the final displacement functions are carried into the expression for the total potential without making any attempt at separating the rigid-body movement. Using this approach, the features classically presented for, including through-the-thickness shear (for example), can be exploited.[12] Smith and Palazotto[13] discussed eight higher-order shear theories to the nonlinear finite element analysis of composite shells. They also used the Green–Lagrange strains and second Piola Kirchhoff stresses. These theories were successful for large displacements and moderately large rotations. A reason for the failure of these theories in the modeling of large rotation can be attributed to the approximations used in the kinematics. Gummadi and Palazotto[14] modified the kinematics incorporated in the SLR theory and successfully carried out the solutions to problems exhibiting the characteristics of very large displacements and rotations. In their work, a vectorial approach was followed to derive the appropriate kinematics that can capture the characteristics of large displacements and large rotations. Using appropriate assumptions, the kinematics for the SLR theory can be obtained as a special case. The large rotation kinematics was introduced through the use of sine and cosine functions. A 36-degree-of-freedom composite shell element was developed based on this theory.

Based on the SLR theory, Tsai and Palazotto[15] formulated a nonlinear dynamic finite element analysis procedure for composite cylindrical shells. In their work, a linear mass matrix was incorporated along with the nonlinear stiffness matrix that was originally developed in SLR theory. This theory again has the same drawbacks as the SLR theory in terms of realizing the large displacements and large rotations. In the present paper, a theory that can capture the large displacement and large rotations is discussed. The present work is an extension of the authors' earlier work on large rotation theory for static analysis. A new mass matrix is generated using Hamilton equations. The mass matrix thus generated is a nonlinear mass matrix. A β–M method[15] is used to solve the nonlinear algebraic equations resulting from the finite element technique. Selected numerical examples are solved to determine the validity of the developed theory.

Theory

Throughout the analysis, the small-strain assumption is used so that the constitutive relationship between Lagrangian stresses and Green strains is assumed to be constant even at large displacements and rotations. A detailed description regarding the derivation of the applicable kinematics that can be used for large kinematics is presented in Ref. 14. Gummadi and Palazotto[14] derived this shell kinematics using a vector format. A normal to the midsurface of a typical shell surface before and after deformation is shown in Fig. 1. In Fig. 1, p is a point on the normal from the midsurface before deformation. Because of the deformation, the position and the orientation of this normal changes and so does the position of the point p on the midsurface. The vectorial difference of the point p on the normal to the midsurface before and after deformation form the desired kinematics. By the use of this approach, the displacement function at any z can be written in global Lagrangian coordinates as

$$u_1 = u + z\sin(\psi_1)\cos(\psi_2)$$

$$u_2 = v[1 - (z/R)] + z\sin(\psi_2)$$

$$u_3 = w + z[\cos(\psi_1)\cos(\psi_2) - 1] \tag{1}$$

Received 7 March 1998; revision received 20 March 1999; accepted for publication 21 April 1999. This paper is declared a work of the U.S. Government and is not subject to copyright protection in the United States.

*Research Associate, Department of Aeronautics and Astronautics. Senior Member AIAA.

†Professor, Department of Aeronautics and Astronautics. Associate Fellow AIAA.

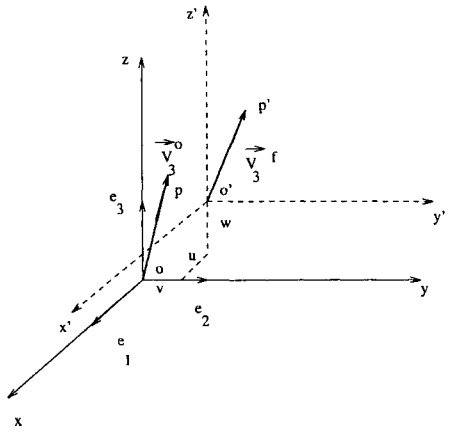

UNDEFORMED AND DEFORMED POSITION VECTORS

Fig. 1 Arbitrary normal of a shell before and after deformation.

where ψ_1 is the angle made by the deformed normal to the original normal in the x–z plane and ψ_2 is the angle made by the deformed normal to the original normal in the y–z plane. These bending angles ψ_1 and ψ_2 are similar to Euler angles for rigid body motion. In Eq. (1), u, v, and w are the displacements of point i on the midplane, and R is the radius of the shell.

It can be observed that by using a small-angle approximation, for both ψ_1 and ψ_2, the basic kinematics used in SLR[11] theory can be obtained. Also, the kinematics used in the SLR theory are based on the third-order shear deformation theory that assumes that the through the thickness shear be parabolic. The present theory is a first-order shear theory that considers a constant through the thickness shear strain. This kinematic assumption violates the zero shear condition on the top and bottom surfaces. However, a shear correction factor of $\frac{5}{6}$ is assumed in computing the energy due to shear toward the development of the stiffness matrix.[14]

Palazotto and Dennis[11] presented explicit expressions for Green strain–displacement relations. To model the cylindrical shell, shell scale factors $h_1 = h_3 = 1$ and $h_2 = 1 - (z/R)$ are used. By using the derived kinematics [Eq. (1)], using Green strain–displacement relations and second Piola Kirchhoff stresses, and incorporating the Hamilton principle, as subsequently discussed, we can obtain the equations of motion as

$$\int_{t_1}^{t_2}\int_A \left\{\{\delta q_2\}^T([\hat{M}]\{\ddot{q}_2\} + [\hat{E}]\{\dot{q}_2\}) + \{\delta q_1\}^T\left(\left[\hat{K} + \frac{\hat{N}_1}{2} + \frac{\hat{N}_2}{3} + \hat{N}_3\right]\{q_1\}\right)\right\} dA\, dt = \int_{t_1}^{t_2}\int_A \{\delta q_1\}^T\{F\}\, dA\, dt \tag{2}$$

where $\{F\}$ is the load vector as a function of time and $\hat{K}$, $\hat{N}_1$, and $\hat{N}_2$ are matrices corresponding to the stiffnesses that are due to strain energy. Of these, $\hat{K}$ is constant, $\hat{N}_1$ is a linear function, and $\hat{N}_2$ is a quadratic function of the displacement gradient vector q_1. The matrix $\hat{N}_3$ is due to the presence of the sine and cosine terms in the kinematics. Here, t_1 and t_2 correspond to the time limits between which preceding equation of motion is valid. A detailed description of the form of these matrices may be found in Refs. 14 and 15. The mass matrix $\hat{M}$ and the artificial damping matrix $\hat{E}$ are functions of the displacement vector q_2 (described subsequently) and are due to the kinetic energy, as seen in the next section.

Development of $\hat{M}$ and $\hat{E}$ Matrices

It is necessary that the expression representing the Hamilton's principle (from a modifed point of view) be carried out, that is,

$$\delta\int_{t_1}^{t_2}(T - \pi + W_{nc})\, dt = 0$$

where T is the kinetic energy, π is the potential energy, and W_{nc} is work of any nonconservative forces. We start from the definition of kinetic energy T, which can be written as

$$\{T\} = \frac{1}{2}\int_v \rho\dot{U}^2\, dv \tag{3}$$

where

$$\{U\}^T = [u_1 \quad u_2 \quad u_3]$$

is the displacement vector shown in the kinematics [Eq. (1)].

The velocity vector $\{\dot{U}\}$ can be written in matrix form as

$$\{\dot{U}\} = [R]\{\dot{q}_2\} \tag{4}$$

where

$$[R] = \begin{bmatrix} 1 & 0 & 0 & 0 & 0 & zS_{11} & zS_{12} \\ 0 & 1 - z/r & 0 & 0 & 0 & 0 & zS_{22} \\ 0 & 0 & 1 & 0 & 0 & zS_{31} & zS_{32} \end{bmatrix}$$

$$[\dot{q}_2]^T = [\dot{u} \quad \dot{v} \quad \dot{w} \quad \dot{w}_{,1} \quad \dot{w}_{,2} \quad \dot{\psi}_1 \quad \dot{\psi}_2]$$

Here, $S_{11} = \cos(\psi_1)\cos(\psi_2)$, $S_{12} = -\sin(\psi_1)\sin(\psi_2)$, $S_{22} = \cos(\psi_2)$, $S_{31} = -\sin(\psi_1)\cos(\psi_2)$, and $S_{32} = -\cos(\psi_1)\cos(\psi_2)$.

It can be shown that by taking the variation of the kinematics [Eq. (1)] and arranging it in a matrix form the expression for the variation of the displacement vector $\{\delta U\}$ can be written as

$$\{\delta U\} = [R]\{\delta q_2\} \tag{5}$$

where

$$[\delta q_2]^T = [\delta u \quad \delta v \quad \delta w \quad \delta w_{,1} \quad \delta w_{,2} \quad \delta\psi_1 \quad \delta\psi_2]$$

By taking the time derivative of $\{\delta U\}$ [Eq. (5)], we can obtain the variation of the velocity vector $\{\delta\dot{U}\}$ as

$$\{\delta\dot{U}\} = [R]\{\delta\dot{q}_2\} + [\dot{R}]\{\delta q_2\} \tag{6}$$

The variation of the velocity vector can also be obtained by taking the variation of the velocity vector $\{\dot{U}\}$ [Eq. (4)]:

$$\{\delta\dot{U}\} = [R]\{\delta\dot{q}_2\} + [\delta R]\{\dot{q}_2\} \tag{7}$$

Thus, from Eqs. (6) and (7), we can write

$$[\delta R]\{\dot{q}_2\} = [\dot{R}]\{\delta q_2\} \tag{8}$$

Note that this is necessary so that any functional variation $([\delta R])$ is related to the displacement vector $\{q_2\}$. The kinetic energy can now be written in terms of the vector $\dot{q}_2$ as

$$T = \frac{1}{2}\int_v \dot{q}_{2(1\times 7)}^T[R]_{(7\times 3)}^T\rho[R]_{(3\times 7)}\{\dot{q}_2\}_{(7\times 1)}\, dv$$

where the subscript $(a \times b)$ indicates the rank of the matrix.

By taking the variation of T and then incorporating Eq. (8), we have the result

$$\delta T = \int_v \left(\delta\dot{q}_2^T\left[[R]^T\rho[R]\{\dot{q}_2\}\right] + \delta q_2^T\left[[\dot{R}]^T\rho[R]\dot{q}_2\right]\right) dv \tag{9}$$

Equation (9) is next transformed into a form that is appropriate for substitution into Eq. (2). This is done by integrating out the $\delta\dot{q}_2$ through the integration by parts technique. The result is

$$\int_{t_1}^{t_2}\delta T\, dt = \int_{t_1}^{t_2}\int_v \delta q_2^T\left[-\frac{\partial}{\partial t}\left([R]^T\rho[R]\dot{q}_2\right) + \left([\dot{R}]^T\rho[R]\right)\dot{q}_2\right] dv\, dt \tag{10}$$

Integrating through the thickness yields

$$\int_{t_1}^{t_2}\delta T\, dt = -\int_{t_1}^{t_2}\int_A \delta q_2^T([\hat{M}]\ddot{q}_2 + [\hat{E}]\dot{q}_2)\, dA\, dt \tag{11}$$

where the mass matrix $\hat{M}$ and the artificial damping matrix $\hat{E}$ are defined as

$$\hat{M} = \int_{-h/2}^{h/2} \rho([R]^T[R])\,dz \tag{12}$$

$$\hat{E} = \int_{-h/2}^{h/2} [R]^T \rho[\dot{R}]\,dz \tag{13}$$

Note that the matrix $\hat{M}$ is symmetric and the matrix $\hat{E}$ can be made symmetric.

The analysis obtained so far is element independent. By the use of this formulation, a 36-degree-of-freedom shell element with four corner nodes and four central nodes (Fig. 2) is developed.

Finite Element Formulation

The shell finite element used for the current formulation is shown in Fig. 2. The element has eight nodes, four corner nodes, and four central nodes. Each corner node has u, v, w, w_x, w_y, ψ_1, and ψ_2, as degrees of freedom, and the central node has u and v as the degrees of freedom (DOF).

The values of the DOF $\boldsymbol{q}(\eta)$ at any point can be expressed in natural coordinates in terms of the element's DOF using the shape functions

$$\boldsymbol{q}_1(\xi, \eta) = T_1\boldsymbol{d}, \qquad \boldsymbol{q}_2(\xi, \eta) = T_2\boldsymbol{d} \tag{14}$$

where the matrices T_1 and T_2 contain the shape functions (of dimension 18×36 and 7×36, respectively) and $\boldsymbol{d}$ is the vector of nodal DOF (a vector of dimension 36×1). Linear shape functions are used for ψ_1 and ψ_2, and quadratic shape functions are used for in-plane displacement variables u, v, and their derivatives, whereas cubic polynomials are used for w and their derivatives.

The derivatives in the displacement vectors $\boldsymbol{q}_1$ and $\boldsymbol{q}_2$ are then transformed from natural coordinates to global coordinates using the inverse of Jacobian matrix, $[J_1]$, $[J_2](\Gamma_1 = J_1^{-1}, \Gamma_2 = J_2^{-1})$, as

$$\boldsymbol{q}_1(x, y) = [\Gamma_1]\boldsymbol{q}_1(\xi, \eta) = [\Gamma_1 T_1]\boldsymbol{d} = [D_1]\boldsymbol{d} \tag{15}$$

$$\boldsymbol{q}_2(x, y) = [\Gamma_2]\boldsymbol{q}_2(\xi, \eta) = [\Gamma_2 T_2]\boldsymbol{d} = [D_2]\boldsymbol{d} \tag{16}$$

If these shape functions are used, the equations of motion can be written as

$$[M]\ddot{\boldsymbol{d}} + [E]\dot{\boldsymbol{d}} + [[K] + ([N_1]/2) + ([N_2]/3) + [N_3]]\boldsymbol{d} - \{F\} = 0 \tag{17}$$

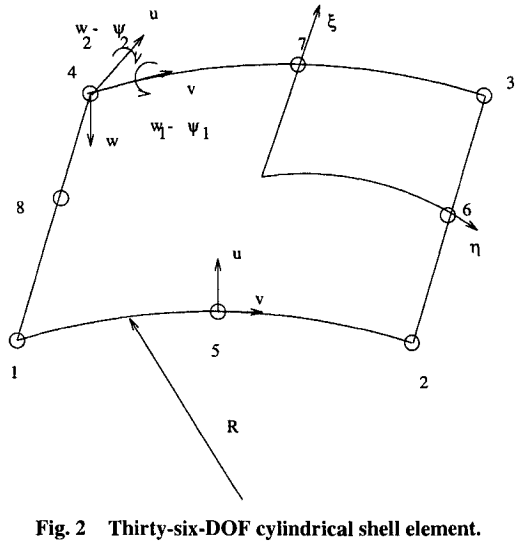

Fig. 2 Thirty-six-DOF cylindrical shell element.

where

$$[M] = \sum \int_{-1}^{1}\int_{-1}^{1} D_2^T \hat{M} D_2\,d\eta\,d\xi$$

$$[E] = \sum \int_{-1}^{1}\int_{-1}^{1} D_2^T \hat{E} D_2\,d\eta\,d\xi$$

$$[K] = \sum \int_{-1}^{1}\int_{-1}^{1} D_1^T \hat{K} D_1\,d\eta\,d\xi$$

$$[N_1] = \sum \int_{-1}^{1}\int_{-1}^{1} D_1^T \hat{N}_1 D_1\,d\eta\,d\xi$$

$$[N_2] = \sum \int_{-1}^{1}\int_{-1}^{1} D_1^T \hat{N}_2 D_1\,d\eta\,d\xi$$

$$[N_3] = \sum \int_{-1}^{1}\int_{-1}^{1} D_1^T \hat{N}_3 D_1\,d\eta\,d\xi$$

$$\{F\} = \sum \int_{-1}^{1}\int_{-1}^{1} D_1^T \hat{F}\,d\eta\,d\xi \tag{18}$$

where the summation is over all of the elements. These nonlinear differential equilibrium equations at each time level can be solved using implicit integration techniques such as the β–M method.

A detailed description of the generalized β–M method may be found in Ref. 15. Here, specific implementation details used for the present formulation are discussed. The β–M method is an implicit integration technique where the dynamic equations of motion at time $n+1$ are used to determine the displacement, velocity, and acceleration at the time $n+1$. Thus, the dynamic equation at the time $n+1$ can be written as

$$M\{\ddot{d}_{n+1}\} + E\{\dot{d}_{n+1}\} + \bar{K}\{d_{n+1}\} = \{F_{n+1}\} \tag{19}$$

It should be recognized that all the matrices, $[M]$, $[E]$, and $[\bar{K}] = [K + N_1/2 + N_2/3 + N_3]$ are nonlinear matrices in terms of the nodal displacement d. The load vector $\boldsymbol{F}$ is a function of time. Using the β–M method (choosing $\beta = 1, m = 0, 1, 2$) the displacement variables at time $n+1$ can be written as

$$\{\ddot{d}_{n+1}\} = \{\ddot{d}_n\} + \{\Delta\ddot{d}\}$$

$$\{\dot{d}_{n+1}\} = \{\dot{d}_n\} + \Delta t\{\Delta\ddot{d}\} + \Delta t\{\ddot{d}_n\}$$

$$\{d_{n+1}\} = \{d_n\} + \{\dot{d}_n\}\Delta t + \{\ddot{d}\}\Delta t^2/2 + \Delta t^2/2\{\Delta\ddot{d}\} \tag{20}$$

Here Δt is the incremental time. Substituting these displacement variables at time $n+1$ into the dynamic equilibrium equation at the time $n+1$,

$$[[M] + [E]\Delta t + [\bar{K}]\Delta t^2/2]\Delta\ddot{d} = \{F_{n+1}\} - [M]\ddot{d}_n$$
$$- [E](\ddot{d}_n\Delta t + \dot{d}_n) - [\bar{K}]\left(d_n + \dot{d}_n\Delta t + \ddot{d}_n\Delta t^2/2\right) \tag{21}$$

These nonlinear algebraic equilibrium equations in terms of the increment $\ddot{d}$ can be solved using the Newton–Raphson methods.

By assuming at each time step that

$$\{\Delta\ddot{d}_{i+1}\} = \{\Delta\ddot{d}_i\} + \{\delta\ddot{d}_i\} \tag{22}$$

where i is the iteration number within a single time step, the algebraic equations can be written as

$$[[M_T] + [E_T] + [K_T]]\{\delta\ddot{d}_i\} = \{F_{n+1}\} - [M]\{\ddot{d}_n + \Delta\ddot{d}_i\}$$
$$- [E]\{\ddot{d}_n\Delta t + \dot{d}_n + \Delta t\Delta\ddot{d}_i\} - [\bar{K}]\left(\{d_n\} + \{\dot{d}_n\}\Delta t\right.$$
$$\left. + \{\ddot{d}_n\}\Delta t^2/2 + \Delta t^2\{\Delta\ddot{d}_i\}\right) \tag{23}$$

where K_T is the tangential stiffness matrix, E_T is the tangential artificial damping matrix, and M_T is the tangential mass matrix. These matrices can be written as

$$[K_T] = [K] + [N_1] + [N_2] + [N_{3T}]$$

$$[M_T] = \sum \int_{-1}^{1} \int_{-1}^{1} [D_2]^T [M^*][D_2]\, d\eta\, d\xi$$

$$[E_T] = \sum \int_{-1}^{1} \int_{-1}^{1} [D_2]^T [E^*][D_2]\, d\eta\, d\xi$$

$$[N_{3T}] = \sum \int_{-1}^{1} \int_{-1}^{1} [D_1]^T [N_3^*][D_1]\, d\eta\, d\xi$$

$$(N_3^*)_{(18\times 18)} = \frac{\partial\{(\hat{N}_3)_{(18\times 18)}(q_1)_{(18\times 1)}\}}{\partial(q_1)_{(18\times 1)}}$$

$$(M^*)_{(7\times 7)} = \frac{\partial\{(\hat{M})_{(7\times 7)}(q_2)_{(7\times 1)}\}}{\partial(q_2)_{(7\times 1)}}$$

$$(E^*)_{(7\times 7)} = \frac{\partial\{(\hat{E})_{(7\times 7)}(q_2)_{(7\times 1)}\}}{\partial(q_2)_{(7\times 1)}} \qquad (24)$$

By solving these incremental equations, we can obtain the global accelerations and, hence, velocities and displacements. The resulting displacement vector is used along with the strain–displacement and constitutive relations to evaluate the stresses at the Gaussian points.

Results and Discussion

The developed element is used to solve a number of arch and shell examples. Dynamic responses under different loading conditions are obtained. Results are compared in precollapse and postcollapse regions with those obtained using earlier attempts in using the total Lagrangian formulation to solve the large displacement and large rotation problems.

Dynamic Response of an Isotropic Cylindrical Shell Under a Sinusoidal Load

The first example considered is a thin, shallow, isotropic cylindrical panel subjected to a uniformly distributed half-sine wave impulsive loading with a peak intensity of 4312.5 Pa (90 psf), as shown in Fig. 3. Geometric dimensions of the shell are shown in Fig. 3. The two straight longitudinal edges of the shell are assumed to be free, and the two curved edges are supported by diaphragms. Material properties of the shell are $E = 20{,}685.4$ MPa ($3.E6$ psi), $\nu = 0$, and weight density = 4312.5 Pa (90 psf). By the consideration of the symmetry, only one-fourth of the panel is modeled using 16 equal elements. The time increment in each load step is taken to be equal to 0.005 s, which is approximately $\frac{1}{25}$ the first natural frequency of the shell. The results are compared to existing results by Clough and Wilson[3] (where through the thickness shear strain is not taken into consideration) and Tsai and Palazotto[15] (where SLR theory is used with through-the-thickness parabolic shear strain). A plot of time vs displacement of point A (Fig. 3) is shown in Fig. 4, where the solid line corresponds to the results obtained from the present theory (using large rotation kinematics with linear through the thickness shear) whereas the dashed line represents the results of Tsai and Palazotto. Results based on Clough and Wilson[3] are shown in circles in Fig. 4. Close agreement can be seen in all three results which is because the transverse shear deformations are small and the rotations and displacements are small. This example validates the accuracy of the developed element and also emphasizes the sufficiency of the much simplified SLR theory when solving the problems of small to moderate rotations and displacements.

Dynamic Analysis of a Laminated Arch Under a Step Load

In the second example, response characteristics of a simply supported laminated arch subjected to a centerpoint load are studied. The analysis is performed on the laminate constructed of AS4-3501-6 graphite epoxy with the following properties: ply thickness = 0.127 mm, $E_{11} = 130{,}000$ MPa, $E_{22} = E_{33} = 10{,}129$ MPa, $G_{12} = G_{13} = 6275$ MPa, $G_{23} = 3100.0$ MPa, $\nu_{12} = 0.28$, $\nu_{21} = \nu_{31} = 0.0218$, and mass density = 0.00242 kg/m^3. The laminate consists of 24 plies with orientation $[0_6/90_6]_s$ in a total thickness of 0.00305 m. As shown in Fig. 5, a radius of curvature of 0.3048 m along with an open angle θ of 1 rad is used. The width of the arch is taken to be the same as the thickness (0.00305 m).

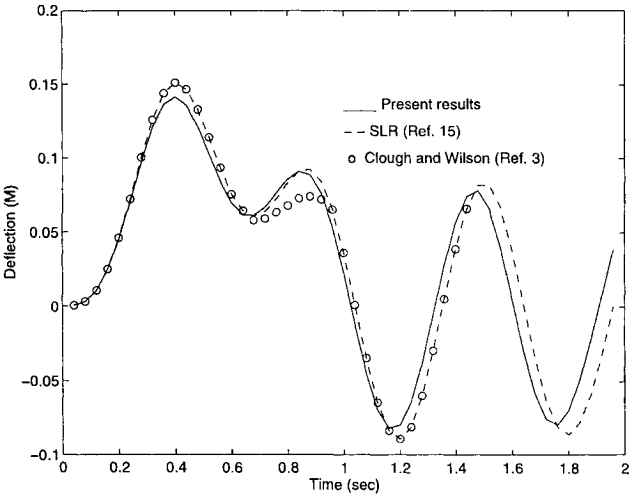

Fig. 4 Dynamic response characteristics of the shallow panel.

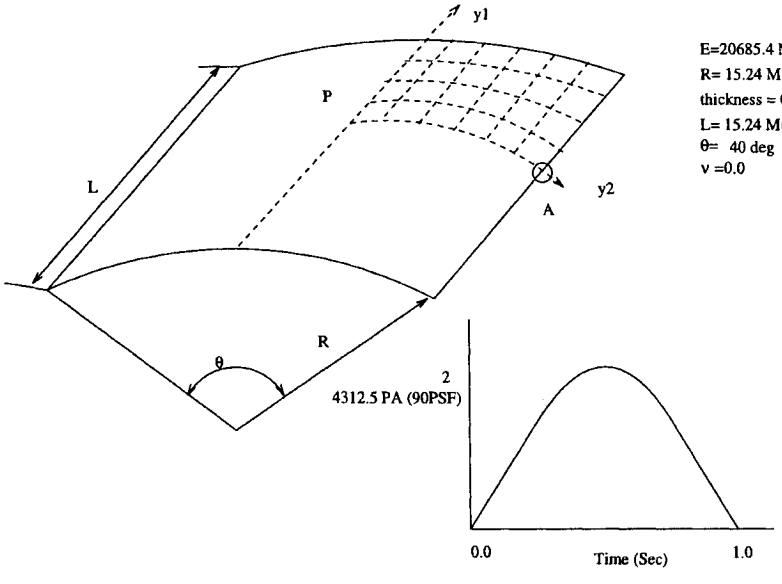

Fig. 3 Geometry and configuration of the cylindrical panel.

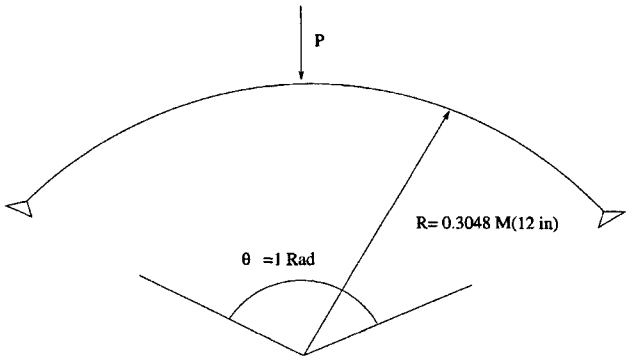

Fig. 5 Geometry and configuration of the laminated arch.

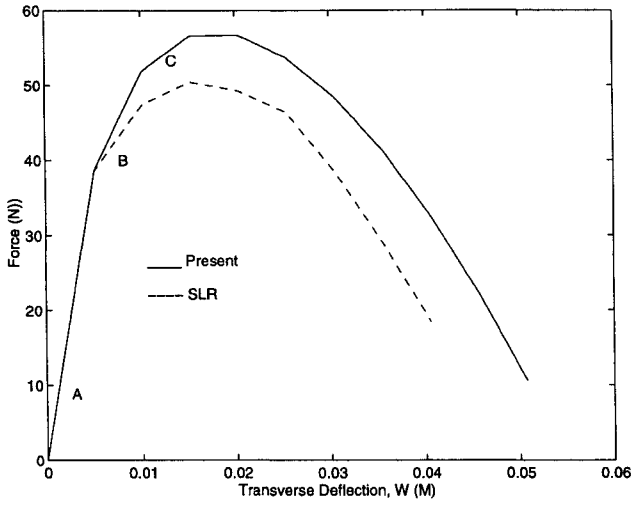

Fig. 6 Static response characteristics of the arch.

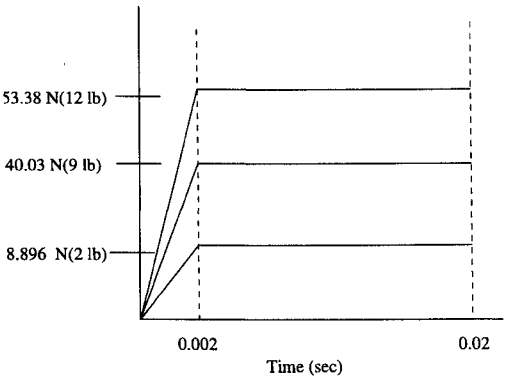

Fig. 7 Loading history for the laminated arch.

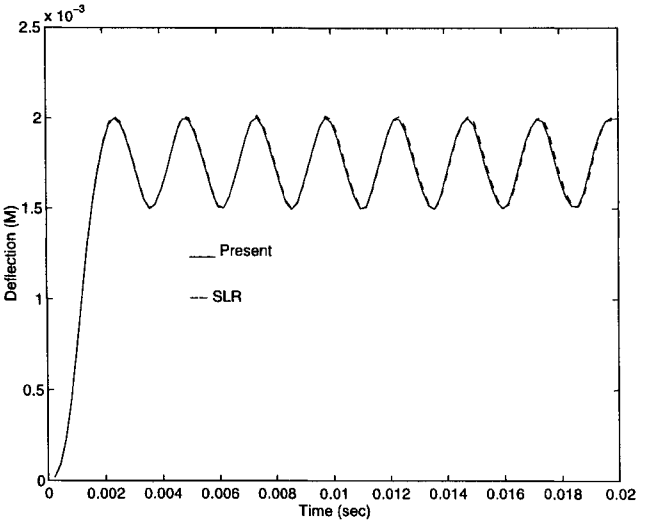

Fig. 8 Dynamic response characteristics of the arch when the peak load is 2 lb.

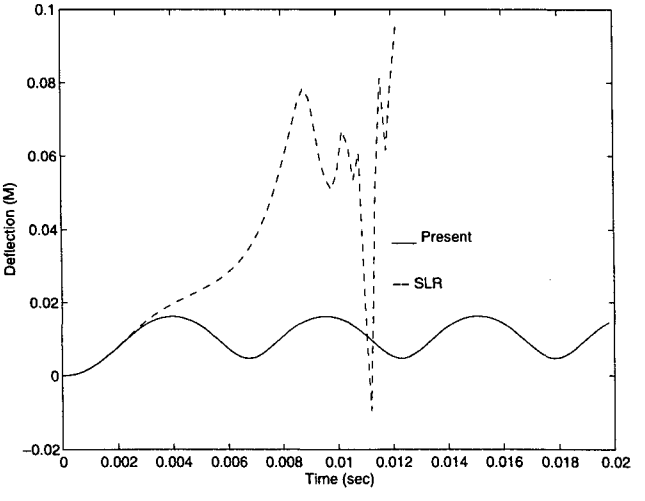

Fig. 9 Dynamic response characteristics of the arch when the peak load is 9 lb.

The arch is modeled as a shell and analyzed using the developed shell element. The two straight longitudinal edges of the shell are assumed to be simply supported, and the two curved circumferential edges are considered to be free. By the utilization of the symmetric nature of the shell (arch), only one-quarter of the shell is modeled using eight shell elements. It was shown by Chien and Palazotto[16] that this arch exhibits the characteristics of snap-through behavior. To understand the snap-through behavior initially, a static analysis is carried out using the present theory and the SLR theory. An increment of 0.00508 m is used in a displacement control approach,[14] and a tolerance of 0.001% is used for convergence between successive iterations within a Newton–Raphson scheme. The results of transverse displacement at the center of the arch as a function of the applied load are compared in Fig. 6, where the solid line corresponds to the present results and the dotted line is the results obtained through SLR theory. Three different regions are identified. Point A is in the interval that corresponds to the precollapse region. Point B is in the interval that describes the collapse region. The region beyond the collapse load is referred as the postcollapse region and point C is in this region. It can be seen from Fig. 6 that the present theory predicts a collapse load of 60 N. Any load below this is in the precollapse region. In the case of the SLR theory, the collapse load corresponds to 51.15 N. That is, there is approximately a 12% difference in the collapse loads predicted by these two theories. For a deeper arch, a much higher difference is observed for the collapse load.[14] It can be seen that the structure based on the present theory always is stiffer than the SLR theory.

The dynamic analysis is carried out for the arch using the β–M method employing cylindrical shell elements using three-step loads with different maximum values as shown in Fig. 7. Each of these maximum loads correspond to the three different regions (precollapse, collapse, and postcollapse). It has been shown by Simitses[8] and Forrel and Palazotto[17] that the dynamic collapse loads are smaller than the static ones, and this was attributed to the presence of inertia terms. Generally, the present authors have observed that the dynamic collapse load is between 80 and 90% of the static collapse load. The maximum load of 8.896 N is in the precollapse region for both theories, the maximum load of 40 N is in the collapse region for the SLR theory (which concurs with the 80–90 precollapse region in the current theory), and the maximum load of 53.38 N (12 lb) is in the postcollapse region for both theories. Results are compared for each of the three loading configurations in Figs. 8–10. The time increment in each load step used is 0.0002 s.

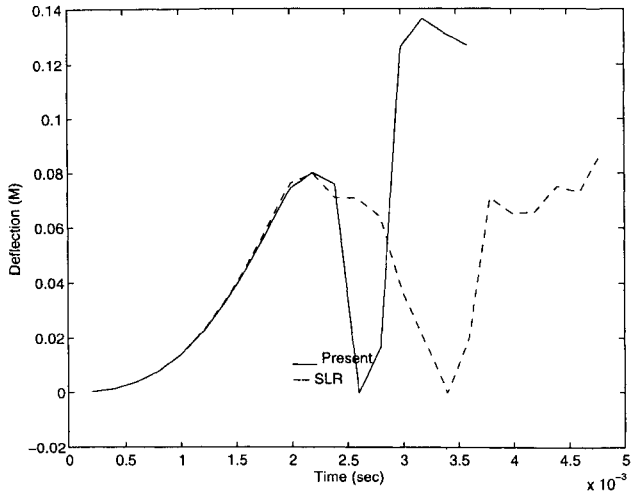

Fig. 10 Dynamic response characteristics of the arch when the peak load is 12 lb.

In Fig. 8, the arch is subjected to a precollapse load. Hence, the dynamic response based on both theories is a smooth periodic vibration. The two theories almost predict the same response characteristics. This agreement in response characteristics is because the arch experiences only small to moderate displacements and rotations, and both theories are the same for such displacements and rotations. In Fig. 9, based on the SLR theory, the arch is subjected to a value close to the collapse load, and hence, a predominantly nonlinear behavior can be seen from these results. However, because this loading is still in the precollapse region based on the present large rotation theory, the response characteristics are observed to be a steady state with periodic oscillations. When the deformation pattern of the arch is observed using the SLR approach, a majority of the arch was found to be experiencing rotations greater than 0.6 rad. At the same load level, based on the current theory, the arch was experiencing a maximum of 0.3 rad. That is, similar to static analysis (as indicated in Gummadi and Palazotto,[18] where a comparison is made to Huddleston's[19] arch solutions), the results based on the current theory are stiffer than the results based on the SLR theory. These differences become significant at larger displacements and rotations. In the third load case, both theories are predicting the arch to be in the postcollapse region, and hence, the response characteristics are observed to have possible chaotic behavior, as indicated by Greer and Palazotto,[20] in both cases as shown in Fig. 10.

Conclusions

A new nonlinear finite element for the dynamic analysis of composite cylindrical shells is developed using a large rotation theory. A nonlinear mass, stiffness matrices, and the β–M method are used to analyze the dynamic response characteristics of shells and arches undergoing moderate to large displacements and rotations. The existing SLR theory is useful when dealing with small to moderate rotations, whereas the current theory is useful when the structure is undergoing large movements. Dynamic instability loading is smaller when compared with the static instability load.

Acknowledgments

The authors acknowledge the financial support received from the U.S. Air Force Office of Scientific Research under Grant F33601-94-CJ026 and Arnold Mayer of Wright Laboratory/FI/Vehicle Subsystems Branch, Wright–Patterson Air Force Base, for this work.

References

[1]Carr, A. J., "A Refined Finite Element Analysis of Thin Shell Structures Including Dynamic Loading," Structural Engineering Lab., Rept. 67-9, Univ. of California, Berkeley, CA, 1967.

[2]Yeh, C. H., "Non Linear Dynamic Analysis of Cooling Tower," *Journal of Power Division, ASCE*, Vol. 98, No. 1, 1972, pp. 49–63.

[3]Clough, W., and Wilson, E. L., "Dynamic Finite Element Analysis of Arbitrary Thin Shells," *Computers and Structures*, Vol. 1, No. 1, 1971, pp. 33–56.

[4]Belytschko, T. B., and Marchertas, A. H., "Nonlinear Finite Element Method for Plates and Its Application to the Dynamic Response of Reactor Fuel Subassemblies," *Journal of Pressure Vessel Technology*, Vol. 96, No. 4, 1974, pp. 251–257.

[5]Belytschko, T. B., and Tsay, C. S., "Explicit Algorithms for Nonlinear Dynamics of Shells," *Nonlinear Finite Element Analysis of Plates and Shells*, edited by T. J. R. Hughes, A. Pifko, and A. Jay, AMD-48, 1981, pp. 209–231.

[6]Saigal, S., and Yang, T. Y., "Nonlinear Dynamic Analysis with a 48 DOF Curved Thin Shell Element," *International Journal of Numerical Methods in Engineering*, Vol. 21, No. 6, 1985, pp. 1115–1128.

[7]Simitses, G. J., *Dynamic Stability of Suddenly Loaded Structures*, Springer-Verlag, Berlin, 1990.

[8]Raouf, R. A., and Palazotto, A. N., "Non-Linear Free Vibrations of Symmetrically Laminated, Slightly Compressed Cylindrical Shell Panels," *Composite Structures*, Vol. 20, No. 4, 1992, pp. 249–257.

[9]Raouf, R. A., and Palazotto, A. N., "Non-Linear Dynamic Response of Anisotropic, Arbitrarily Laminated Shell Panels: An Asymptotic Analysis," *Composite Structures*, Vol. 18, No. 2, 1991, pp. 163–192.

[10]Simo, J. C., and Tarnow, N., "A New Energy and Momentum Conserving Algorithm for the Nonlinear Dynamics of Shells," *International Journal for Numerical Methods in Engineering*, Vol. 37, 1994, pp. 2527–2549.

[11]Palazotto, A. N., and Dennis, S. T., *Nonlinear Analysis of Shell Structures*, AIAA, Washington, DC, 1992.

[12]Reddy, J. N., "A Simple Higher-Order Theory for Laminated Composite Plates," *Journal of Applied Mechanics*, Vol. 51, No. 4, 1984, pp. 745–752.

[13]Smith, R. A., and Palazotto, A. N., "Comparison of Eight Variations of a Higher-Order Theory for Cylindrical Shells," *AIAA Journal*, Vol. 31, No. 6, 1993, pp. 1125–1132.

[14]Gummadi, L. N. B., and Palazotto, A. N., "Total Lagrangian Approach to Nonlinear Finite Element Analysis of Cylindrical Shells Considering Large Rotations," *Proceedings of the AIAA/ASME/ASCE/AHS 37th Structures, Structural Dynamics, and Materials Conference*, AIAA, Reston, VA, 1996, pp. 2034–2043.

[15]Tsai, C. T., and Palazotto, A. N., "On the Finite Element Analysis of Non-Linear Vibration for Cylindrical Shells with High-Order Shear Deformation Theory," *International Journal of Nonlinear Mechanics*, Vol. 26, No. 14, 1991, pp. 379–388.

[16]Chien, L. S., and Palazotto, A. N., "Dynamic Buckling of Composite Cylindrical Panels with High Order Transverse Shears Subjected to a Transverse Concentrated Load," *International Journal of Nonlinear Mechanics*, Vol. 27, No. 5, 1992, pp. 719–734.

[17]Forrel, A. E., and Palazotto, A. N., "A Finite Element Model Considering Nonlinear Dynamically Loaded Composite Plates and Shells," *International Journal for Engineering Analysis and Design*, Vol. 1, 1994, pp. 379–394.

[18]Gummadi, L. N. B., and Palazotto, A. N., "Nonlinear Analysis of Beams and Arches Undergoing Large Rotations," *Journal of Engineering Mechanics*, Vol. 123, No. 4, 1997, pp. 394–398.

[19]Huddleston, J. V., "Finite Deflections and Snap Through of High Circular Arches," *Journal of Applied Mechanics*, Vol. 35, No. 4, 1968, pp. 763–769.

[20]Greer, J. M., and Palazotto, A. N., "Nonlinear Dynamics of Simple Shell Model with Chaotic Snapping Behavior," *Journal of Engineering Mechanics*, Vol. 121, No. 6, 1995, pp. 753–761.

G. A. Kardomateas
Associate Editor